Am J Transl Res 2023;15(7):4678-4686
www.ajtr.org /ISSN:1943-8141/AJTR0149644

Original Article

Application of magnetic resonance neuroimaging in determining the relationship between tumors and peripheral nerves

Chaochao Wang*, Lihui Fu*, Liang Liang, Jinlong Zhou

*Department of Radiology, Li Huili Hospital of Ningbo Medical Center, Ningbo 315041, Zhejiang, P. R. China. *Equal contributors and co-first authors.*

Received February 13, 2023; Accepted June 26, 2023; Epub July 15, 2023; Published July 30, 2023

Abstract: Background: Magnetic resonance imaging (MRI) is commonly used to analyze the relationship between tumors and nerves before surgery. However, the application value of diffusion tensor imaging (DTI), diffusion weighted imaging (DWI), and post-processing techniques needs further elucidation. Purpose: To assess the value of DTI, DWI, and various post-processing techniques in determining the relationship between tumors and nerves. Material and Methods: The participants were 42 patients diagnosed with peripheral nerve-related tumors and 20 healthy controls. DTI and DWI scans were performed before surgery, and then DTI unidirectional maximum intensity projection (MIP) post-processing and DWI subtraction of unidirectionally encoded images for suppression of heavily isotropic objects (DWI_{SUSHI}) postprocessing techniques were used to observe the relationship between the mass and the target nerves. The mean apparent diffusion coefficient (ADC) of nerves was compared among the target neural origin group, non-target neural origin group, and healthy control group using the paired Wilcoxon rank-sum test. Results: The diagnostic coincidence rates of preoperative DTI and DWI findings with postoperative pathology were 88.1% and 100%, respectively. DTI images were of poor quality when compared to DWI_{SUSHI} ($P < 0.05$). The mean ADC value of the target neural origin group was greater than that of the non-target neural origin group and the healthy control group ($P < 0.05$). Conclusion: Both DTI and DWI_{SUSHI} can stereoscopically display the relationship between peripheral nerves and tumors, but the latter contributes to better quality of the reconstructed images.

Keywords: Magnetic resonance imaging, diffusion tensor imaging, diffusion-weighted imaging, peripheral nerve

Introduction

Peripheral nerve-related tumors are either of the neural origin or of non-neural origin [1, 2]. Tumors of neural origin, such as schwannomas and neurofibromas, are mostly benign [3, 4], while those of non-neural origin are mainly tumors originating from muscles, blood vessels, bones, etc. around the nerves, causing compression on the nerves [5, 6]. Removal of peripheral nerve-related tumors requires high surgical precision. On the contrary, inadvertent nerve injury during surgery may lead to irreversible dysfunction in patients, such as sensory loss and loss of motor function [7]. Therefore, it is necessary to comprehensively understand the relationship between the tumor and the nerves before surgery to avoid nerve damage during the procedures.

For the preoperative evaluation of peripheral nerve-related tumors, traditional methods mainly rely on indirect evaluations, such as physical and electrophysiological examinations of symptoms and signs [8]. On this basis, the visualization of the morphological relationship between the tumor and the target nerve would provide valuable insights, which would be instructive for the formulation of surgical plans. Magnetic resonance imaging (MRI) is recognized as the preferred method to study peripheral nerve morphology due to its high soft tissue resolution and various functional imaging and post-processing techniques [9]. In this study, based on the anisotropic characteristics of nerves, diffusion tensor imaging (DTI), diffusion weighted imaging (DWI) and various post-processing techniques were used to display the whole picture of peripheral nerves and tumors

in three dimensions, so as to determine the relationship between peripheral nerves and tumors before surgery in a non-invasive and accurate manner.

Material and methods

Participants

Retrospectively, 62 subjects admitted from January 2017 to December 2021 were selected for analysis, including 42 patients with peripheral nerve-related tumors diagnosed by clinical and routine MRI examinations and 20 healthy controls. Inclusion criteria: (1) patients presented numbness and weakness of the limbs innervated by the relevant nerves, or experienced atrophy of the innervated skeletal muscles; (2) patients showed abnormal motor or sensory branches in the innervation of the target peripheral nerve (i.e., the parent nerve of the tumor of peripheral nerve origin or the nerve of non-peripheral origin but compressed by the tumor) in electromyography; (3) patients did not have contraindications to MRI; (4) patients underwent imaging using a 3-T MRI scanner; (5) patients had complete imaging results and clear images; (6) patients did not undergo any invasive treatment before MRI scanning; (7) patients underwent surgical resection within two weeks after the MRI examination and obtained pathological results. Exclusion criteria: (1) patients presented with contraindications to MRI (e.g., implanted pacemaker, cochlear implants, claustrophobia); (2) patients had incomplete imaging results and unclear images. The healthy control group consisted of 12 males and 8 females, with a median age of 42 years (range: 28-62). There was no significant difference in general data such as sex and age between the two groups (all $P > 0.05$). In each of the 5 tumor sites, 4 healthy controls were for the same sequence of DTI and DWI scans. This retrospective study was approved by the institutional review board and ethics committees of the Li Huili Hospital of Ningbo Medical Center. Patient consent was waived by the ethics committee due to the retrospective nature of the study.

Imaging acquisition

All patients were examined using a 3-T MRI scanner (Discovery MR 750; GE Medical Systems, Milwaukee, WI, USA). With the corresponding coil selected, the target joint of the patient lying in a comfortable position was immobilized and placed in the center of the magnet. The scan range was about 5-10 cm above and below the lesion. The scanning sequence consisted of 25 directional DTI sequences and 2 unidirectional DWI sequences, which represent the anterior-posterior (AP) and superior-inferior (SI) directions of the diffusion gradient, respectively. The spin echo-echo plane imaging sequence was used for DTI scanning. The scanning parameters were as follows: repetition time (TR): 8000 ms, echo time (TE): 92 ms, number of layers: 40-58 layers, layer thickness: 2 mm, layer spacing: 0 mm, excitation times: 4, flip angle: 90°, plane reconstruction matrix: 256 × 256, dispersion coefficient b value: 1000 s/mm^2, and number of scanning dispersion directions: 25. DWI used echo plane imaging sequence and axial AP direction (DWI_{AP}), with the direction of diffusion sensitive gradient selected as AP direction and the scanning parameters set as follows: TR: 4000 ms, TE: 63.10 ms, bandwidth: 1953 Hz/Px, field of view: 28, flip angle: 90°, excitation times: 18, b value: 800 s/mm^2, slice thickness: 3 mm, and slice spacing: 0 mm; the direction of axial SI (DWI_{SI}): all parameters and scanning positioning were consistent with DWI_{AP}, and the SI direction was selected the diffusion sensitive gradient.

The images obtained were transferred to a workstation (Advantage Workstation 4.5; GE Medical Systems) and then processed independently by two neuroradiologists (with 15 and 20 years of neurological MRI experience) with no knowledge of the participants' information. In the DTI sequence, the original data perpendicular to the nerve orientation were selected for maximum intensity projection (MIP) reconstruction, and observed at any angle in parallel. DWI_{AP} and DWI_{SI} were subtracted from the original data to generate a new sequence DWI_{SUSHI} (subtraction of unidirectionally encoded images for suppression of heavily isotropic objects, SUSHI). DWI_{SUSHI} data were reconstructed by MIP and viewed from any angle in parallel. In cases of some high signal noises (such as veins, lymph nodes), these noises were removed to facilitate the observation of nerves.

Image quality assessment

The DTI and DWI_{SUSHI} MIP reconstructed images of the 42 included patients were evaluated sub-

Table 1. Comparison of general information

General information	Patient group (n=42)	Healthy control group (n=20)	χ^2/t	P
Sex (male/female)	27/15	12/8	0.107	0.744
Age (years old)	46.31 ± 17.67	46.95 ± 12.30	0.146	0.885
Weight (kg)	65.64 ± 10.36	64.60 ± 10.82	0.364	0.717
Tumor site (elbow/brachial plexus/wrist/hip)	18/10/10/4	-		
Skeletal muscle atrophy (yes/no)	4/58	-		
Drinking history (yes/no)	16/26	5/15	1.037	0.309
Smoking history (yes/no)	18/24	7/13	0.348	0.556

jectively and quantitatively. The scoring scale was developed with reference to the research design scheme of Zhao et al. [10], which evaluated the ability of the imaging method to stereoscopically display the target nerve and mass, as well as the intensity of nerve signals. The scale has a score range of 0-3 points: 0 point: the target nerve and mass are not clearly displayed and cannot be distinguished; 1 point: the target nerve and mass can be fully displayed with weak nerve signal intensity; 2 points: the target nerve and mass can be completely displayed, with good nerve signal intensity; 3 points: the target nerve and mass can be completely displayed, with excellent nerve signal intensity. The denoising effect was assessed based on the amount and distribution of noise, with a score range of 0-4 points [11]: 0 points: the noise mixes with nerves that results in the inability to identify nerves; 1 point: there is a lot of scattered noise, which if not removed, will affect the nerve reading; 2 points: the noise is relatively concentrated and would affect the neural reading due to occlusion when rotated to a certain angle; 3 points: there is a little more noise, but would not influence neural image reading even if it is not removed; 4 points: there is very little noise that can affect neural image reading. Two senior diagnostic imaging physicians randomly and independently reconstructed MIP images for all patients, and the image quality was scored and recorded.

Measurement and comparison of apparent diffusion coefficient (ADC) of target nerves

Using workstation post-processing software, ADC values were measured on raw DWI_{AP} images of all the 62 subjects in this study. Multiple regions of interests (ROIs) were plotted manually for measurement. The range of ROI was selected to include the largest possible section of the nerve without exceeding the actual nerve range. Six measurements were made within the range of 1-2 cm above and below the target nerve lesion area for each patient, and the mean was recorded. In the healthy control group, the target nerves within the scanning range were measured using the same method.

Statistical analysis

All statistical analyses were performed by SPSS software (version 22.0, SPSS, Chicago, IL, USA). Non-normally distributed measurement data, expressed as the median, were compared between groups using the paired Wilcoxon rank-sum test. The normally distributed measurement data were expressed as $\bar{x} \pm s$, and the t test was used for comparison between groups. Kappa analysis was used for consistency evaluation, with Kappa value < 0.4, 0.4 ≤ Kappa value ≤ 0.6, 0.6 < Kappa value ≤ 0.8, and 0.8 < Kappa value ≤ 1.0 indicating poor, medium, good, and very good consistency, respectively. The ADC values between the patient group and the healthy control group were compared using the two independent samples t-test. Differences of $P < 0.05$ were considered statistically significant.

Results

Comparison of general information

As shown in **Table 1**, the patients and controls showed no statistical differences in sex, age, weight, drinking history, smoking history and other general information ($P > 0.05$).

Preoperative diagnosis coincidence rates of two different scanning and post-processing methods

According to the postoperative pathological diagnosis of the 42 tumor patients, 32 cases

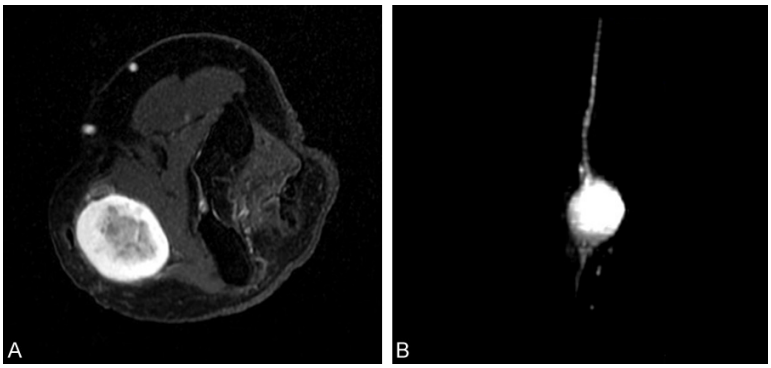

Figure 1. A 66-year-old female patient with a schwannoma of the median nerve at the right elbow. A. On the axial T2WI fat-suppressed image, a mixed hyperintense mass was found in the right elbow median nerve course. B. On the DWI_{SUSHI} MIP reconstruction image, the mass was connected to the median nerve, and the preoperative diagnosis of schwannoma of the median nerve was consistent with the postoperative pathology. DWI: Diffusion weighted imaging, MIP: maximum intensity projection.

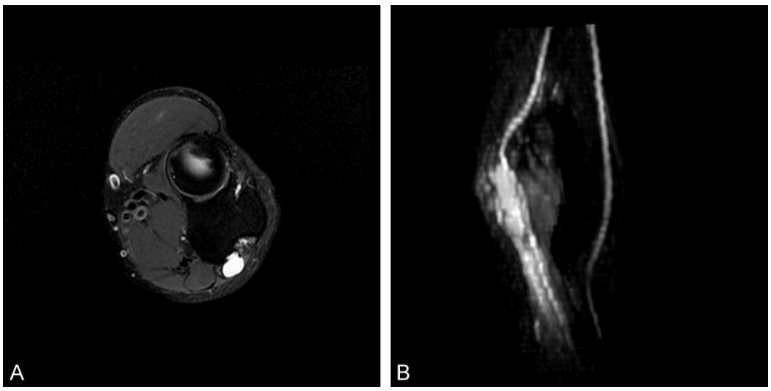

Figure 2. A 56-year-old male patient with a synovial cyst in the ulnar nerve region of the right elbow. A. The axial T2WI fat-suppressed image showed a cystic mass in the ulnar nerve course. B. According to the DWI_{SUSHI} MIP reconstruction image, the mass was adjacent to the ulnar nerve, which could be fully displayed, and there was a gap between the masses. The preoperative diagnosis of the cystic mass was of non-ulnar nerve origin, which was consistent with the pathology. DWI: Diffusion weighted imaging, MIP: maximum intensity projection.

were of peripheral nerve origin (19 cases of schwannomas, 8 cases of neurofibromas, and 5 cases of malignant neurofibromas) and 10 cases were of non-peripheral nerve origin (2 cases of fibroids, 1 case of osteochondroma, 4 cases of hemangioma, and 3 cases of cyst). Preoperative DTI determined 31 tumors of target peripheral nerve origin, 6 tumors of non-target peripheral nerve origin, and 5 tumors of unknown origin. The coincidence rate of preoperative DTI diagnosis with postoperative pathological diagnosis was 88.1%. The preoperative DWI determined that the tumor originated from the target peripheral nerve in 32 cases and from the non-target peripheral nerve in 10 cases, with a coincidence rate with postoperative control pathological diagnosis of 100% (**Figures 1**-**3**).

Image quality assessment results

The MIP reconstructed DWI_{SUSHI} images of the patients were all of good quality, with favorable denoising effects, which could display the target nerve and mass in 3D while clearly distinguishing the relationship between lesions and nerves. However, the background noise in the MIP reconstructed images of unidirectional DTI was relatively large, and the target nerves were difficult to distinguish in 5 patients due to noise interference, resulting in the inability to determine the relationship between the lesion and the nerves. The two post-processing methods, DWI_{SUSHI} and DTI, showed whether nerves and masses were displayed throughout the process and the mean signal intensity score, as well as the denoising effect score. The two techniques were in good agreement between the two measures, with the Kappa values of 0.804 and 0.845, respectively, as shown in **Table 2**. The MIP reconstruction images of DWI_{SUSHI} were significantly better than unidirectional DTI in terms of whether the nerve was fully displayed, and the difference was statistically significant ($P < 0.05$).

Comparison of ADC values between groups

The mean ADC values of the target neural origin group, non-target neural origin group, and healthy control group were $(1.81 \pm 0.124) \times 10^{-3}$ mm^2/s, $(1.24 \pm 0.087) \times 10^{-3}$ mm^2/s, and

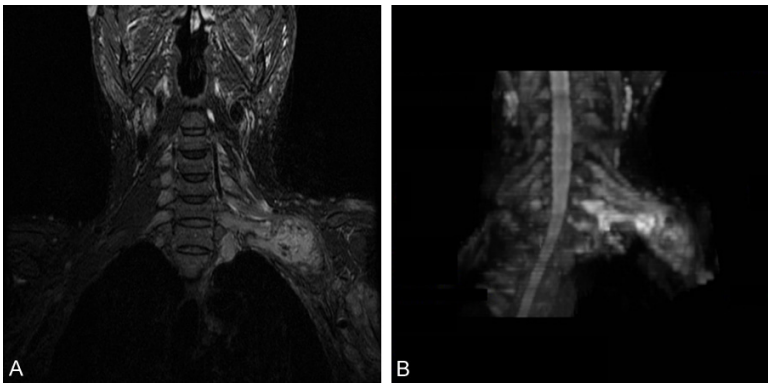

Figure 3. A 52-year-old man with malignant schwannoma of the left brachial plexus. A. On the axial T2WI fat-suppressed image, there was proximal thickening of the left multiple brachial plexus and a mass with mixed T2WI signal. B. The DWI_{SUSHI} MIP reconstruction image showed the destruction of the brachial plexus in the mass area, which was unclear. It was diagnosed preoperatively as a malignant tumor of brachial plexus origin, which was consistent with the pathological diagnosis. DWI: Diffusion weighted imaging, MIP: maximum intensity projection.

(1.22 ± 0.102) × 10^{-3} mm^2/s, respectively (**Figure 4**). There was a statistically significant difference in the ADC value between the target nerve origin group and the healthy control group ($P < 0.01$), and between the target neural origin group and the non-target neural origin group ($P < 0.05$). While no significant difference was identified between the non-target nerve origin group and the healthy control group ($P > 0.05$).

Discussion

MRI, characterized by non-invasiveness and high resolution, has been widely used in the diagnosis and postoperative follow-up of peripheral nerve injury, entrapment, tumor and other lesions [12-14]. The principle of DTI is based on the anisotropic diffusion motion of water molecules in nerves [15]. Under normal physiological conditions, water molecules in nerves are limited by microstructures such as nerve myelin sheaths, with the diffusion speed of water molecules perpendicular to the nerve direction being much lower than that of water molecules parallel to the nerve direction. Peripheral nerve injury can lead to stretched or neurogenic tumors, resulting in varying degrees of nerve fiber damage and Wallerian degeneration [16, 17]. Due to the destruction of the internal environment of the nerve, the diffusion of water molecules loses their anisotropic properties. While DTI can stereoscopically display the morphological changes of nerves by detecting the microscopic changes in the Brownian motion of water molecules in all directions [16, 18].

DTI is long in scanning time (generally more than 20 directions need to be collected) and cumbersome in post-processing operations [19]. It requires layer-by-layer tracking down markers to achieve stereoscopic imaging of fiber bundles, and is difficult to accurately track smaller nerves. Therefore, scholars have been exploring a simple and objective reconstruction method. Skorpil et al. [20] applied the MIP post-processing method to reconstruct the original image of a single direction obtained by the DTI scan of the sciatic nerve, and automatically obtained the neural stereo image. They found that the neural signal was the strongest after reconstruction of the data perpendicular to the direction of the nerve, and the weakest after the reconstruction of the DTI data parallel to the direction of the nerve. In this study, DTI scan images in 25 directions were collected and the raw data perpendicular to the nerve direction were selected for MIP reconstruction to automatically generate 3D stereo images. The target nerves and masses showed high signals, and the surrounding tissues such as blood vessels and lymph nodes were also hyperintense in the magnetic field due to limited diffusion, so the background noise around the nerves was heavier. However, the depiction of the nerve was almost unaffected because these structures are usually not adjacent to the nerve and can be easily removed by post-processing, or can be separated from the nerve by rotating a different projection [10]. Thus, manual denoising is required to facilitate 3D and multi-angle observation. Preoperative DTI determined that the tumor originated from the target nerve in 31 cases and non-target nerve in 6 cases, while the tumor origin remained undetermined in 5 cases due to heavy noise and the inability to fully display the nerves and masses. The diagnostic coincidence rate of preoperative DTI with post-

Table 2. Neuroimaging quality assessment results

Score	DTI	DWI_{SUSHI}	Kappa value	*P* value
Whether the nerve is displayed throughout the process and the signal intensity score	1.25 (1, 1.5)	2.5 (2, 3)	0.804	< 0.05
Denoising effect score	2.5 (1.5, 3)	4.0 (4, 4)	0.845	< 0.05

DTI: Diffusion tensor imaging, DWI: diffusion weighted imaging.

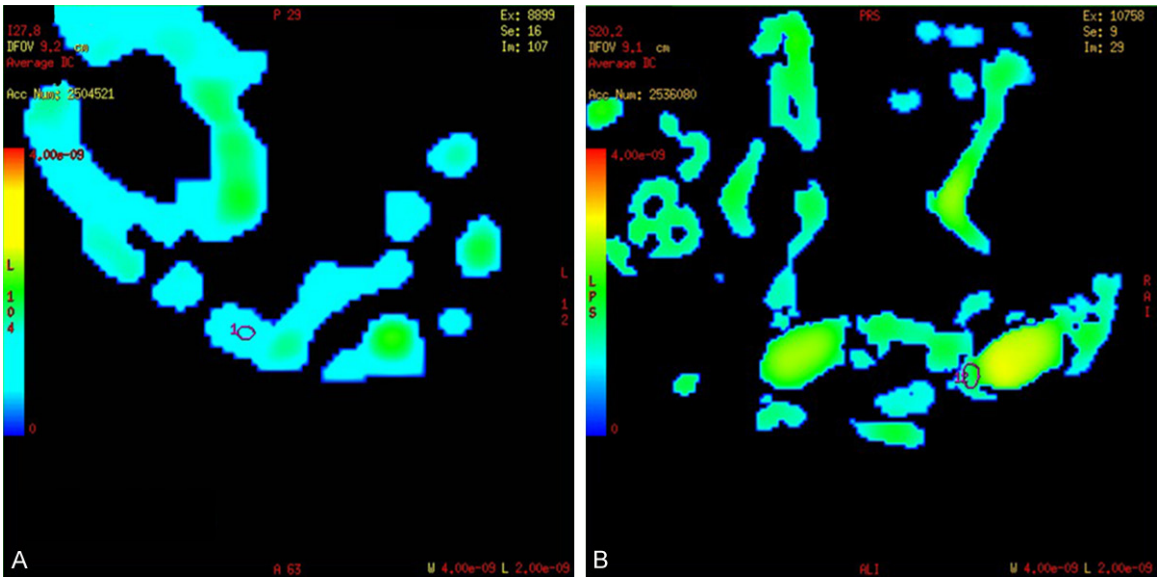

Figure 4. The ADC map of the ulnar nerve at the elbow in a healthy control and a patient. A. A 38-year-old male healthy control with an ADC value of 1.1 × 10^{-3} mm^2/s. B. A 67-year-old male patient with an ulnar schwannoma of the left elbow: there was a mass connected to the ulnar nerve with an ADC value of 1.67 × 10^{-3} mm^2/s.

operative pathology was 88.1%. The 5 patients with severe image noise in this group were all elder patients. We believe that the patients are suffering from subtle motion artifacts caused by the discomfort of a fixed position for a long time in DTI, which affects image quality.

DWI can select several diffusion sensitive gradient directions, shorten the scanning time, and appropriately increase the number of acquisitions, so that high-quality and high-signal-to-noise 3D reconstructed images can be obtained in a relatively short time [21]. Peripheral nerves are highly anisotropic structures with significant diffusion limitations in their vertical plane and facilitated diffusion along their main axis [20]. These physiological features allow the use of DWI to study peripheral nerves, lumbar or brachial plexus nerves. Takahara et al. [22] created a new post-processing method based on DWI, and named it SUSHI. The AP direction and the SI direction parallel to the body axis are collected to obtain the DWI_{AP} and DWI_{SI} data, respectively. DWI_{AP} data are subtracted from DWI_{SI}, and the obtained data are DWI_{SUSHI}, while MIP reconstruction of DWI_{SUSHI} can present a stereoscopic image containing only nerves. In the DWI_{AP} images, both the nerves and the surrounding tissues show high signals; while the nerves in DWI_{SI} images present low signal intensity, and the signal values of the surrounding tissues are close to those of DWI_{AP}. Due to the significantly higher anisotropy level of nerves compared to surrounding tissues, the diffusion level of water molecules is significantly higher than that of surrounding tissues. After the two are subtracted, most of the background noise around the nerve can be automatically removed, and the remaining noise becomes loose and not connected to the nerve, making the target nerve and mass clearly visible. In this study, this method was used to determine the relationship between the mass and the nerve before surgery, with a coincidence rate of 100% compared with postoperative pathology.

In addition, the DWI_{AP} data of 20 healthy subjects and 42 patients were used to measure ADC values using workstation post-process-

ing software. The ADC value can reflect the Brownian motion ability of water molecules in the nerve, with a higher ADC value suggesting a stronger diffusion ability of water molecules in the nerve. ADC may be useful to confirm and quantify the presence of edema in peripheral nerves trauma or compression and to characterize tumor lesions [23, 24]. The target nerves in the healthy control and non-neural origin groups were structurally intact, and the diffusion movement of water molecules in the AP direction was weaker, so the average ADC value was lower. It was observed that the patients in the neural origin group had neuro-Wallerian degeneration due to structural destruction of nerve fibers or prolonged compression [25]. As a result, water molecules lose the confinement of microstructures, such as myelin sheaths, leading to enhanced diffusion strength and elevated mean ADC values. ADC is generated by the difference in the signal intensity term between low and high *b* values. ADC reflects the displacement of water molecules in the extracellular space, regardless of the movement direction of the water molecules [26]. High ADC values are consistent with this increase in extracellular space and usually represent edema regardless of its source (i.e., trauma, compression, or fiber breakage). Therefore, the ADC value can not only intuitively reflect the presence or absence of nerve damage, but also quantify the injury degree, which can be applied to non-invasive monitoring of peripheral nerve damage and postoperative repair [24, 27].

In this study, the above two scanning and reconstruction methods were used, both of which were found to be able to clearly and three-dimensionally display the target nerve and mass. In the evaluation of image quality, DTI unidirectional MIP reconstruction images were found to be inferior to DWI_{SUSHI} in terms of display of nerves and masses throughout the process, signal intensity score, and denoising effect. This is attributed to the heavier background noise. Namely, the MIP reconstruction image quality of DWI_{SUSHI} is better, contributing to clearer and more accurate preoperative display of nerves and lesions. Furthermore, the DWI scan time was short (about 6 minutes in total for 2 acquisitions), which takes only about half of the time required for DTI. Thus, patients have less discomfort due to prolonged body position fixation, and scan failures caused by patient motion artifacts are more likely to be avoided. The benign tumors of neural origin were mainly neurofibromas or schwannomas (19 cases in this group), both of which present MRI features of benign tumors. However, schwannomas are prone to cystic degeneration inside the mass, and the MRI signal is often uneven. On DTI and DWI three-dimensional images, schwannomas are mostly located on the lateral side of the nerve (eccentricity), while neurofibromas are mainly manifested as the parent nerve passing through it, showing the “nerve entry and exit sign”. In 5 cases of malignant neurofibromatosis or fibromatosis, the tumor signals were mixed, resulting in the inability to distinguish the nerves within the tumor-bearing segment due to structural damage. In the other 10 cases of non-neural origin masses, the running of the target nerve, the signal, and the ADC value were normal, and the mass and the target nerve were clearly demarcated by a certain distance.

The shortcomings of this study are that the MR coil is not optimized and the sample size is small, warranting the inclusion of more cases in the future to explore optimized MRI neuroimaging and post-processing methods. For MR coil optimization, there are various approaches, such as (1) selecting a coil unit that matches the scan site, (2) increasing the field of view as appropriate, and (3) using filtering techniques. Of course, the exact approach depends on the cause of artifact formation.

Conclusion

In conclusion, the MIP reconstructed images of DTI and DWI_{SUSHI} enable a three-dimensional and intuitive display of the peripheral nerves, which is of great value for preoperative determination of the relationship between peripheral nerves and tumors. There is a very high rate of coincidence between preoperative DTI and DWI diagnosis and postoperative pathological diagnosis. DWI_{SUSHI} has great advantages in clinical practice due to the excellent quality of the reconstructed images and the short scanning time, leading to improved work efficiency.

Acknowledgements

Zhejiang Medical and Health Science and Technology Plan Project, Project No. 2020-KY856.

Disclosure of conflict of interest

None.

Address correspondence to: Lihui Fu, Department of Radiology, Li Huili Hospital of Ningbo Medical Center, Ningbo 315041, Zhejiang, P. R. China. Tel: +86-0574-87018807; E-mail: 13857405407@163.com

References

[1] Farma JM, Porpiglia AS and Vo ET. Benign neurogenic tumors. Surg Clin North Am 2022; 102: 679-693.

[2] Luna R, Fayad LM, Rodriguez FJ and Ahlawat S. Imaging of non-neurogenic peripheral nerve malignancy-a case series and systematic review. Skeletal Radiol 2021; 50: 201-215.

[3] Dai A and Cai JP. Intravascular schwannoma: a review of a rare diagnosis. J Cutan Pathol 2021; 48: 314-317.

[4] Mo J, Anastasaki C, Chen Z, Shipman T, Papke J, Yin K, Gutmann DH and Le LQ. Humanized neurofibroma model from induced pluripotent stem cells delineates tumor pathogenesis and developmental origins. J Clin Invest 2021; 131: e139807.

[5] Cage TA, Yuh EL, Hou SW, Birk H, Simon NG, Noss R, Rao A, Chin CT and Kliot M. Visualization of nerve fibers and their relationship to peripheral nerve tumors by diffusion tensor imaging. Neurosurg Focus 2015; 39: E16.

[6] Gersing AS, Cervantes B, Knebel C, Schwaiger BJ, Kirschke JS, Weidlich D, Claudi C, Peeters JM, Pfeiffer D, Rummeny EJ, Karampinos DC and Woertler K. Diffusion tensor imaging and tractography for preoperative assessment of benign peripheral nerve sheath tumors. Eur J Radiol 2020; 129: 109110.

[7] Kaul V and Cosetti MK. Management of vestibular schwannoma (including NF2): facial nerve considerations. Otolaryngol Clin North Am 2018; 51: 1193-1212.

[8] Martín Noguerol T, Barousse R, Gómez Cabrera M, Socolovsky M, Bencardino JT and Luna A. Functional MR neurography in evaluation of peripheral nerve trauma and postsurgical assessment. Radiographics 2019; 39: 427-446.

[9] Jang H and Du J. Optimizing diffusion-weighted mri of peripheral nerves. Radiology 2022; 302: 162-163.

[10] Zhao L, Wang G, Yang L, Wu L, Lin X and Chhabra A. Diffusion-weighted MR neurography of extremity nerves with unidirectional motion-probing gradients at 3 T: feasibility study. AJR Am J Roentgenol 2013; 200: 1106-1114.

[11] Bao H, Wang S, Wang G, Yang L, Hasan MU, Yao B, Wu C, Zhang X, Chen W, Chan Q, Wu L and Chhabra A. Diffusion-weighted MR neurography of median and ulnar nerves in the wrist and palm. Eur Radiol 2017; 27: 2359-2366.

[12] Manzanera Esteve IV, Farinas AF, Pollins AC, Nussenbaum ME, Cardwell NL, Kahn H, Does MD, Dortch RD and Thayer WP. Noninvasive diffusion MRI to determine the severity of peripheral nerve injury. Magn Reson Imaging 2021; 83: 96-106.

[13] Li H, Li Z, Li Q, Mei L, Pierre BS, Abdullenur A, Huang T, Wang W, Mao X and Zhu W. Arthroscopic management of giant meniscal cysts among young patients: an average three-year MRI follow-up. Orthop Surg 2022; 14: 1743-1750.

[14] Aman M, Schwarz D, Stolle A, Bergmeister KD, Boecker AH, Daeschler S, Bendszus M, Kneser U and Harhaus L. Modern MRI diagnostics of upper-extremity-related nerve injuries-a prospective multi-center study protocol for diagnostics and follow up of peripheral nerve injuries. J Pers Med 2022; 12: 1548.

[15] Holmes SA, Staffa SJ, Karapanagou A, Lopez N, Karian V, Borra R, Zurakowski D, Lebel A and Borsook D. Biological laterality and peripheral nerve DTI metrics. PLoS One 2021; 16: e0260256.

[16] Chiou SY, Hellyer PJ, Sharp DJ, Newbould RD, Patel MC and Strutton PH. Relationships between the integrity and function of lumbar nerve roots as assessed by diffusion tensor imaging and neurophysiology. Neuroradiology 2017; 59: 893-903.

[17] Liang W, Han B, Hai Y, Yin P, Chen Y and Zou C. Diffusion tensor imaging with fiber tracking provides a valuable quantitative and clinical evaluation for compressed lumbosacral nerve roots: a systematic review and meta-analysis. Eur Spine J 2021; 30: 818-828.

[18] Chianca V, Albano D, Messina C, Cinnante CM, Triulzi FM, Sardanelli F and Sconfienza LM. Diffusion tensor imaging in the musculoskeletal and peripheral nerve systems: from experimental to clinical applications. Eur Radiol Exp 2017; 1: 12.

[19] Awais K, Snoj Ž, Cvetko E and Serša I. Diffusion tensor imaging of a median nerve by magnetic resonance: a pilot study. Life (Basel) 2022; 12: 748.

[20] Skorpil M, Engström M and Nordell A. Diffusion-direction-dependent imaging: a novel MRI approach for peripheral nerve imaging. Magn Reson Imaging 2007; 25: 406-411.

[21] Sagiyama K, Watanabe Y, Kamei R, Baba S and Honda H. Comparison of positron emission tomography diffusion-weighted imaging (PET/DWI) registration quality in a PET/MR

scanner: zoomed DWI vs. conventional DWI. J Magn Reson Imaging 2016; 43: 853-858.
[22] Takahara T, Kwee TC, Hendrikse J, Van Cauteren M, Koh DM, Niwa T, Mali WP and Luijten PR. Subtraction of unidirectionally encoded images for suppression of heavily isotropic objects (SUSHI) for selective visualization of peripheral nerves. Neuroradiology 2011; 53: 109-116.
[23] Eguchi Y, Ohtori S, Yamashita M, Yamauchi K, Suzuki M, Orita S, Kamoda H, Arai G, Ishikawa T, Miyagi M, Ochiai N, Kishida S, Masuda Y, Ochi S, Kikawa T, Takaso M, Aoki Y, Toyone T, Suzuki T and Takahashi K. Clinical applications of diffusion magnetic resonance imaging of the lumbar foraminal nerve root entrapment. Eur Spine J 2010; 19: 1874-1882.
[24] Martín Noguerol T, Barousse R, Socolovsky M and Luna A. Quantitative magnetic resonance (MR) neurography for evaluation of peripheral nerves and plexus injuries. Quant Imaging Med Surg 2017; 7: 398-421.
[25] Song M, Kang K and Song F. SARM1-mediated wallerian degeneration: a possible mechanism underlying organophosphorus-induced delayed neuropathy. Med Hypotheses 2021; 155: 110666.
[26] Anderson AW, Xie J, Pizzonia J, Bronen RA, Spencer DD and Gore JC. Effects of cell volume fraction changes on apparent diffusion in human cells. Magn Reson Imaging 2000; 18: 689-695.
[27] Keller S, Wang ZJ, Golsari A, Kim AC, Kooijman H, Adam G and Yamamura J. Feasibility of peripheral nerve MR neurography using diffusion tensor imaging adapted to skeletal muscle disease. Acta Radiol 2018; 59: 560-568.